Solvent design aiming at solution property induced surface stability: a case study using SiC solution growth

Xinbo Liu[a], Yifan Dang[a], Koki Suzuki[a], Can Zhu[a], Wancheng Yu[a], Shunta Harada[a,b], Miho Tagawa[a,b], Toru Ujihara[a,b,c]

[a] *Department of Materials Process Engineering, Nagoya University, Furo-cho, Chikusa-ku, Nagoya, 464-8603, Japan*
[b] *Center for Integrated Research of Future Electronics (CIRFE), Institute of Materials and Systems for Sustainability (IMaSS), Nagoya University, Furo-cho, Chikusa-ku, Nagoya, 464-8601, Japan*
[c] *GaN Advanced Device Open Innovation Laboratory (GaN-OIL), National Institute of Advanced Industrial Science and Technology (AIST), Furo-cho, Chikusa-ku, Nagoya, 464-8601, Japan*

Abstract

For solution growth of silicon carbide, it is significant to understanding the evolutionary mechanism of step bunching. This study infers that solute's incorporation into steps and transport together determines step bunching progress. The occurrence of step bunching is due to the depletion of solute in the region with high step density, caused by a high step kinetic coefficient. On the other hand, by promoting the transport of the solute in the solution, the step speed becomes uniform, thereby the step bunching can be prevented. Furthermore, we proposed a non-dimensional Damköhler number for crystal growth in step-flow mode. It correlates incorporation rates with bulk diffusion rates and can build a phase map of growth rates and step bunching stability. Several solvents are located in the phase map, demonstrating the possible usage of the phase map as a pointer for solvent designing.

Keywords: A1. CFD, A1. Diffusion, A1. Step kinetic coefficient A1. Step bunching, A2. Solvent,

Email address: x-liu@unno.material.nagoya-u.ac.jp (Xinbo Liu)

1. Introduction

Silicon carbide, especially its 4H-polytype, has proven to be a promising material for next-generation power devices due to its excellent physical properties, such as its wide bandgap, high thermal conductivity, high electric breakdown voltage, and large saturated drift velocity. [1, 2] Solution growth is a potential method for producing high-quality bulk SiC crystals since growth processes under conditions close to thermal equilibrium. [3] We have reported dislocations in seed SiC crystals being converted and wiped out during solution growth. [4, 5, 6, 7, 8] By utilizing the threading dislocation conversion phenomenon, we demonstrated crystals of dramatically high quality.[9] The total dislocation density has been lowered to 200 cm^{-2}, which is a close value to the result obtained by the repeated *a*-face growth (RAF) growth process.[10]

Since the liquid phase at the composition of SiC is not available, a so-called self-flux method based on silicon melt is utilized. In this method, carbon dissolves at the graphite-solvent interface, transport through diffusion and convection in solution, and crystallizes on the seed crystal. However, the negligible solubility of carbon in pure silicon melt limits the growth rate to a low level. The Si-Cr binary solvent has been extensively studied. The addition of chromium increases the growth rate while suppresses the formation of 2D nucleation. Because the supersaturation, $\Delta c = c - c_{\mathrm{eq}}$, the driving force of growth, is enhanced, while the relative supersaturation, $\sigma = \Delta c / c_{\mathrm{eq}}$, the driving force of nucleation, is reduced, respectively. [11, 12, 13, 14]

Besides the enhancement of growth rate and suppression to 2D nucleation, the solvent composition also affects the surface morphology during the so-called step-flow growth carried out on the vicinal surface. Step bunching is a typical unfavorable morphology due to the following inclusion and dopant inhomogeneity. [15, 16] The addition of a small amount of aluminum has been proved effective in suppressing step bunching and thus improving the growth morphology of SiC by Mitani et al.[14, 17, 18] With an in-situ observation of the step motions at the growing SiC crystal, Onuma et al. pointed out that step bunching is suppressed due to a change made by adding Al in surface kinetics rather than in mass transportation. [19] Additive elements can thus be utilized to modify the step to a demanded height and shape for specific purposes. We revealed the effect on step morphology of silicon-titanium solvent during growth 4H-SiC on the C face. [20, 21] Afterwards, Si-5%Ti solvent has been utilized to modify the shape of steps on the C

face of 4H-SiC to realize threading dislocations' conversion. [22] In addition to experiments, theoretical studies are focused on illuminating the mechanism of solution properties affecting step morphology. [23, 24] Mitani et al. compared the growth results of 19 different additive elements and concluded that additive elements change the interface energies; thus, two-dimensional nucleation rates vary. However, the mechanism in which additive elements affecting step bunching behavior remains open to discussion. [25]

A general understanding of the step bunching mechanism is essential for solvent design. However, it remains challenging because the mechanism includes an interplay between mass transport and surface kinetics. In this study, we constructed a computational fluid dynamics (CFD) model coupling the physical phenomena at the growth interface and focused on the role of solute transport and surface kinetics in step growth rate and bunching behavior. We come to a similar conclusion as the Mullins-Sekerka instability but address the kinetic perspective of step bunching.

2. Computer simulations

In this study, a fluid dynamics simulation coupling with surface kinetics is carried out to investigate how physical properties affect surface stability. This model is inspired by the similar works done previous researchers.[26, 27, 28] Only we combined the features of 1) multiple steps in one grid [26] and 2) calculate step velocities post solute concentration[27, 28] This model allows us to simulate the behavior of plenty of steps without increasing mesh density. Values of the step kinetic coefficient $\mathcal{K}_{\mathrm{st}}$ and diffusion coefficient $\mathcal{D}$ are changed, and step velocities and positions are observed to quantify growth rate and bunching behavior.

The diagrammatic illustration of the model is shown in Figure 1. The model contains a solution part and a surface part. The solution part describes the mass transport and absorption of growth units in a laminar boundary layer near the crystal. The upper boundary of the solution part ($y = y_{\max}$) indicates the interface between the laminar boundary layer and the imaginary bulk solution. While the surface part, located at the bottom boundary of the solution part, mimics a vicinal surface where aligned steps train advancing. As shown in Fig.1 (b, c), the surface part are divided into grids (the X_is). The step motion is independent of the grids. However, when a step enters one mesh, it will maintain the same velocity as the other steps in this mesh. (Fig.1 (d))

Note that we did not explicitly consider the step height in the calculation of mass transport because the step height is minor compared with the length scale of the solution. [26] However, since the top of a bunch protrudes to the solution, a bunch-top step should be less affected than a bunch-bottom step by the solute depression caused by the step bunch. Although this difference may be minor, we consider it significant at the initial stage of the instability. One will find that some step bunches are artificially created to introduce instability, and the step bunches have symmetrical profiles. One will also find the step velocity related to the profile. That means step movements in the two sides of a bunch, that is, entering and leaving the bunch, corresponding to bunching and de-bunching, are supposed to be symmetrical, as well. It is the above-mentioned minor difference between the top and bottom steps that broke the symmetry and led to instability. Before de-bunching, a bottom step must move in the mesh containing the bunch at a relatively small velocity due to the depression caused by the bunch. On the other hand, a step moves faster before it enters the mesh, and once it crosses the mesh border, it gets bunched. That leads to a fast bunching than de-bunching in the simulation, yet the bunch profile is symmetrical.

2.1. Model formulation

The solute transport in the solution volume is described by the convection-diffusion equation of the form

$$\frac{\partial c}{\partial t} + \mathbf{v} \cdot \nabla c = \mathcal{D} \nabla^2 c. \tag{1}$$

The boundary condition at top of the fluid domain where $y = \delta_c$, is set as

$$c = c_\infty, \tag{2}$$

where c_∞ is the bulk concentration in solution. The horizontal boundaries are set to be periodical. According to the mass conservation, the boundary condition at the solution-solid interface is formulated for each boundary mesh as:

$$N \overline{v_{\mathrm{st}}} \rho^{\mathrm{S}} h = \mathcal{D} \left. \frac{\partial \rho^{\mathrm{L}}}{\partial y} \right|_{y=0} \Delta x, \tag{3}$$

Where N is the number of steps in a mesh, ρ^{S} and ρ^{L} are the solutal density in solid and liquid phase, respectively. Δx is the mesh size in x-direction, $\overline{v_{\mathrm{st}}}$ is the mean velocity of the steps in the mesh and h is the step height.

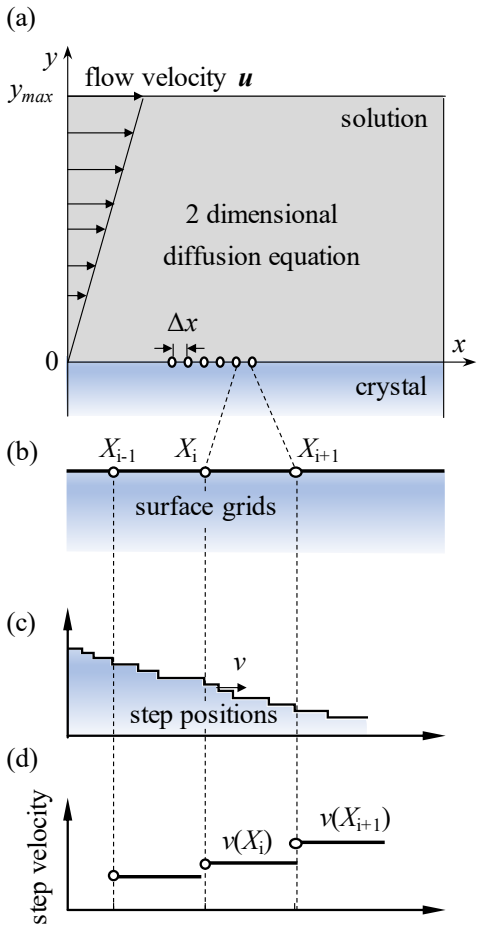

Figure 1: The schematic diagram of the model. (a)shows the components of solution and crystal surface. (b)shows the diagram of grids on the surface. (c)is a schematic diagram of the actual stepped vicinal surface corresponding to the configuration of crystal surface in the simulation, and (d)shows the calculated step velocities in each grid.

In grids with zero steps in, the boundary condition eq. 3 becomes a simple Neumann boundary condition

$$\frac{dc}{dy} \equiv 0. \tag{4}$$

A step's velocity can to be calculated with the concentration near the step, c_{st}, with [29]

$$v_{\mathrm{st}} = \mathcal{K}_{\mathrm{st}} v_{\mathrm{c}} (c_{\mathrm{st}} - c_{\mathrm{eq}}), \tag{5}$$

where $\mathcal{K}_{\mathrm{st}}$ is the step kinetic coefficient and v_{c} is the volume of growth unit, which is considered to be 1/4 of the 4H-SiC primitive cell. Combine the molar concentration and the volume of growth unit then we get

$$v_{\mathrm{st}} = \mathcal{K}_{\mathrm{st}} (c^*_{\mathrm{st}} - c^*_{\mathrm{eq}}), \tag{6}$$

where $c^* = c \times v_{\mathrm{c}}$. And since $\rho^{\mathrm{L}}/\rho^{\mathrm{S}}|_{y=0} = c^*_{\mathrm{st}}$, the boundary condition can be written as

$$Nh\mathcal{K}_{\mathrm{st}} (c^*_{\mathrm{st}} - c^*_{\mathrm{eq}}) = \mathcal{D} \frac{\partial c^*_{\mathrm{st}}}{\partial y} \Delta x. \tag{7}$$

2.2. Determination of physical parameters

The diffusion coefficient of carbon in pure silicon melt can be calculated with [30]

$$\mathcal{D} = 7.55 \times 10^8 \exp(\frac{-9150}{1.9856T}) \ [\mu \mathrm{m}^2/\mathrm{s}]. \tag{8}$$

Since the solubility of carbon in pure silicon melt is small, consider the density of carbon's silicon solution being the same as pure silicon melt with

$$\rho = 2.54 - 1.59 \times 10^{-4}(T - T_m) - 1.15 \times 10^{-7}(T - T_m)^2 \ [\mathrm{g/cm}^3], \tag{9}$$

where T is the temperature and T_m is the melting point of silicon. The carbon solubility in pure silicon melt can be calculated in mole fraction with [31]

$$a\% = \exp(\frac{-2.97 \times 10^4}{T} + 7.95). \tag{10}$$

Converted in weight fraction

$$w\% = \frac{1}{1 + \frac{M_{Si}}{M_C}(\frac{1}{a\%} - 1)} \tag{11}$$

and converted to molar concentrationin

$$c = \rho \frac{w\%}{M_C} N_A \times 10^{-12} \ [\text{mole}/\mu\text{m}^3]. \tag{12}$$

where M is the molecular weight, N_A is the Avogadro number. While the normalized concentration c^* appeared in this study is the number of solutal atoms in every primitive cell

$$c^* = c \times v_\text{c}, \tag{13}$$

where $v_\text{c} = 2.0554 \times 10^{-11} \mu\text{m}^3$ is the volume of a primitive cell of 4H-SiC.

The physical properties used in simulations shown in Figure 3, 4 and 5 are listed in Table 1 while the properties for simulation shown in Figure 6 are listed in Table 2. The physical properties used for simulation shown in Figure 7 and 8 are the same as those listed in Table 1 except the varied values of diffusion coefficient and step kinetic coefficient.

3. Results and discussion

3.1. Effects of $\mathcal{K}_\text{st}$

Primarily, the step velocity is directly determined by the step kinetics, which is characterized by the step kinetic coefficient. It is defined as

$$\mathcal{K}_\text{st} = \nu a_\text{st} (\frac{a_\text{k}}{\delta_\text{k}}) \exp(-\frac{\Delta U}{k_B T}), \tag{14}$$

where ν is the attempt frequency, a_st is the unit advancing distance of a step, a_k and δ_k are the length of a single kink site and the average distance between two neighbouring kink sites, respectively. ΔU is the solvation barrier, k_B is the Boltzmann constant and T is the temperature. In the pre-exponential factor, δ_k, the average distance between kinks, can be written as $\delta_\text{k} = a[1 + 1/2 \exp(\omega/k_B T)]$, where ω is the energy necessary for creation of a kink,[32] which is actually the interface energy of the crystal-solution interface in our case. Thus we consider the step kinetic coefficient reflecting an important aspect of the solution properties.

One of the major obstacles to fully linking experimentally observed step bunching behaviors to additive elements is our lack of knowledge about the step kinetics. Onuma et al. indicated that the transition from step bunching to stable growth by addition of aluminum is due to surface kinetics rather

Table 1: Physical properties used in simulation for revealing the effect of step kinetic coefficient.

Physical property	Mark	Value	Unit
Boundary condition			
Step height	h	3.0730	Å
Off angle	θ	0.75	$\circ$
Equilibrium concentration	c^*_{eq}	0.00188	
Bulk concentration	c^*_{∞}	0.00476	
Geometry			
x-direction length	L_x	40	μm
y-direction length	L_y	300	μm
Initial Configuration			
Pertubation wave number	k_x	π	$\mu\mathrm{m}^{-1}$
Pertubation amptitude	δ_x	0.1	μm
Dynamics			
Temperature	T	2073	K
Diffusion coefficient	$\mathcal{D}$	8180	$\mu\mathrm{m}^2/\mathrm{s}$
Step kinetic coefficient	$\mathcal{K}_{\mathrm{st}}$	2×10^0 - 2×10^7	μm/s

Table 2: Physical properties used in simulation for revealing the effect of diffusion coefficient.

Physical property	Mark	Value	Unit
Boundary condition			
Step height	h	3.0730	Å
Off angle	θ	0.75	∘
Equilibrium concentration	c^*_{eq}	1.0	
Bulk concentration	c^*_{∞}	2.0	
Geometry			
x-direction length	L_x	50	μm
y-direction length	L_y	50	μm
Dynamics			
Diffusion coefficient	$\mathcal{D}$	10^4 & 10^8	$\mu\mathrm{m}^2/\mathrm{s}$
Step kinetic coefficient	$\mathcal{K}_{\mathrm{st}}$	10^4 & 10^8	μm/s

than other solution properties like diffusivity or carbon solubility. Although the direct evidence for step kinetics being modified by aluminum is not able to be obtained, they convincingly conducted the conclusion through two facts, with the addition of 5% aluminum, the thermal calculation showing that solvent properties change minorly and the step velocities showing a transition from a step height dependant mode to a step height independent mode. [19] However, a direct and quantitative study is still necessary to reveal the influence of kinetics on step bunching. Experimentally determining the step kinetic coefficient (as the fraction of step velocity and supersaturation) requires an *in-situ* measurement to elementary steps, which is very difficult, if not impossible, in the case of solution growth of SiC for the high growth temperature. In this study, therefore, we carried out a series of simulations with a varied $\mathcal{K}_{\mathrm{st}}$ values to reveal its influence on step bunching behavior.

The simulations are carried out on a 0.75° tilted vicinal substrate. Thus the surface is intrinsically stepped. Figure 2 shows the diagram of the side view of a stepped surface. The line graph indicates the surface with step trains perfectly equidistant arranged, with the n-th step's "perfect position" being $n\delta_0$. The steps advance towards the x-direction in v_{st}. To introduce an instability, we set steps deviating from the perfect positions by $\delta_x \cos(kn\delta_0)$ in the initial simulation configuration, indicated by the filled graph. This

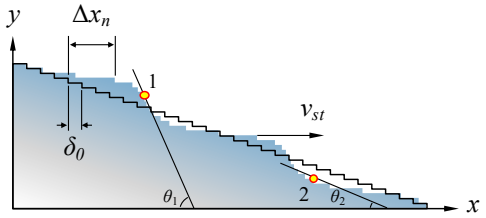

Figure 2: The schematic diagram of the vicinal surface. Evenly spaced step trains are represented by a line graph, while step trains deviating from evenly spaced positions by $\delta_x \cos(kn\delta_0)$ are represented as a filled graph. The deviation of step position leads to steps aggregating and separating periodically, forming a periodically step-bunching morphology. The numbers indicate regions with different step densities.

initial configuration is the same ones in step bunching analyses utilizing the perturbation theory.[33, 34, 35, 36] Since it is difficult to affirm whether an elementary step is bunched, the "local slope" is measured instead in this study. On a smooth surface, each step has the same local slope of $p_0 = \tan\theta_0$, where θ_0 is usually mentioned as the "off-angle" in experimental studies. On an undulated surface, the local slope varies. For a step in a step bunching (indicated as 1 in Fig.2) it is $p_1 = \tan\theta_1$ while for a step out of a bunching (indicated as 2) it is $p_2 = \tan\theta_2$, where $\theta_1 > \theta_2$ are the angles between the tangent line of surface profile passing the step and the horizontal line. We can quantitatively tell how dense the step is bunched by measuring the elementary step's local slopes. Table 1 lists the other parameters used in the simulation.

Figure 3 shows (a) the initial and (b) the as-grown surface morphology. Note that this is an enlarged portion of the whole surface with a total length of 40 μm. Compared with the initial morphology, the step bunchings on the as-grown surface are higher and steeper. The statistic root-mean-square (RMS) of the surface height measures the surface roughness.

$$\Delta h_{\mathrm{RMS}} = \sqrt{\frac{1}{n}(\Delta h_1)^2 + (\Delta h_2)^2 + ... + (\Delta h_n)^2}, \tag{15}$$

where Δh_i is the difference between the i-th interpolated value on the surface height profile and the mean surface height. Fig.3(b) diagramticly shows the measurement of Δh_i and the mean surface height.

The changes of surface roughnesses over time are measured for two crystals with step kinetic coefficients varying from 2μm/s to $2 \times 10^7 \mu$m/s. We

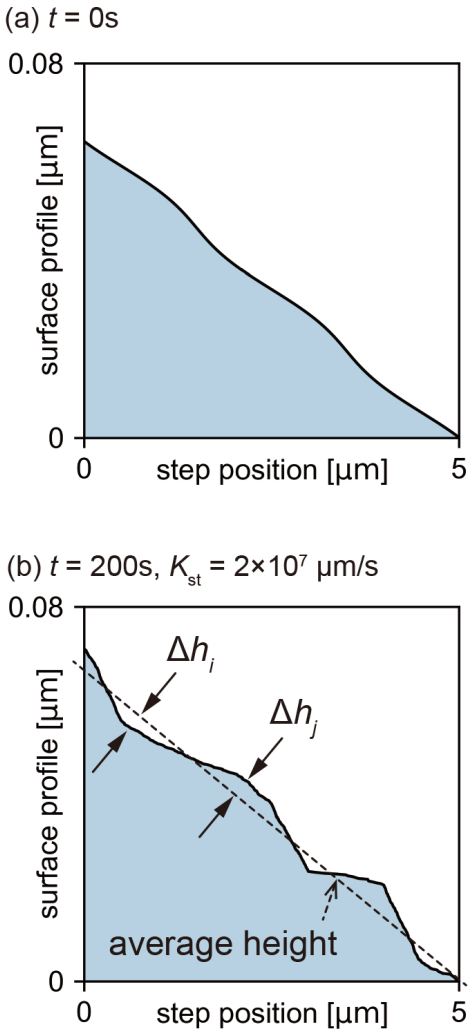

Figure 3: The enlarged height profile of the crystal surface (a)before and (b)after growth. The growth period is 500 seconds.

chose such a wide range because the $\mathcal{K}_{\rm st}$ can vary broadly when the temperature, kink creation work, or the solvation barrier are changed. The results $\mathcal{K}_{\rm st} = 2 \times 10^7 \mu$m/s and $2 \times 10^3 \mu$m/s are shown in Figure 4. The rest results show no significant difference from the results obtained with the two values. For the clarity of our discussion, only the two critical results are displayed. The growth time at maximum is 500 seconds. Because no artificial solid-on-solid (SOS) restriction is applied in this model and the steps in the case of $\mathcal{K}_{\rm st} = 2 \times 10^7 \mu$m/s starts to overlap after growing for over 500s. (Although an SOS restriction is usually preferred for the advantage of preventing steps from overlapping, we did not include the restriction due to a consideration of the law of mass conservation.) For the crystal with a small value of $\mathcal{K}_{\rm st} = 2 \times 10^3 \mu$m/s, the surface roughness remains constant, indicating there is little further step bunching. While for the crystal with a large value of $\mathcal{K}_{\rm st} = 2 \times 10^7 \mu$m/s, the surface roughness increases exponentially over time with a short-period oscillation. The reason for the exponential growth will be discussed in the next section. The oscillation and increase of surface roughness imply how steps bunch. Once step bunches are formed, the elementary steps are not constantly fixed in the current bunches. Instead, the elementary steps keep leaving their current bunches from the front and entering the next bunches from behind. This results in two kinds of temporary states, 1) there are more elementary steps leaving than entering, and the step bunches dissipate, 2) there are more entering than leaving, and the step bunches grow. It is the alternating of the two temporary states which leads to the oscillation in surface roughness. If the entering of elementary steps to bunches is faster than leaving, the probability of temporary state 1) thus is higher than 2). Therefore, the step bunches are enhanced, and the surface roughness increase. That is the exact reason why would a large value of kinetic coefficient results in step bunching.

To vertify the mechanism of $\mathcal{K}_{\rm st}$ affecting step bunching behavior, the step velocities $v_{\rm st}$ against the local slopes p are plotted in Figure 5. Note that the local slope p is replaced with step the local density

$$p_{\rm i} = \frac{N_{\rm i}}{\Delta x}, \tag{16}$$

where the subscript i refers to the i-th surface grid and N is the number of steps in the surface grid. According to the mechanism of step bunching, a step bunch increases its height because the steps in it have different velocities from the other steps. As shown in Fig.5(a), despite the variance among

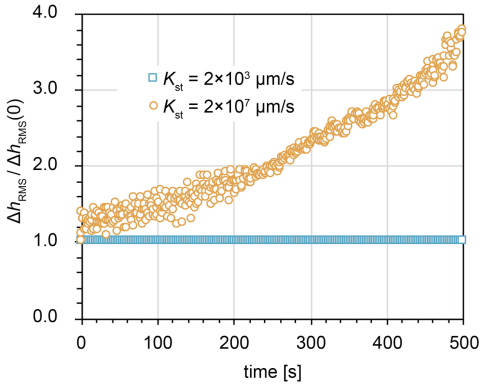

Figure 4: Change of surface roughnesses over growth time. Note that the root mean square of height profile is normalized by its initial value for clear.

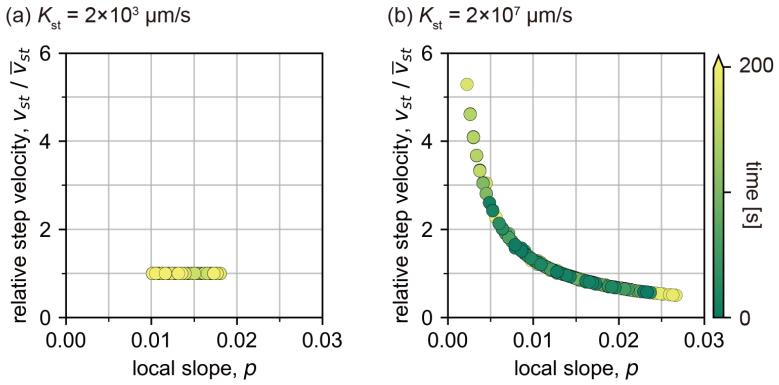

Figure 5: Scatter plots of step velocities against the local slopes over the growth time of crystal whose step kinetic coefficient is (a)$2 \times 10^3 \mu$m/s (b)$2 \times 10^7 \mu$m/s. The scatters colors indicate the time passed since the growth started.

local slopes, step velocities are the same and remain constant over the whole growth duration. Bear in mind that the step's local slope indicates how dense the step is bunched. The constant and slope-independent velocities reveal that with small $\mathcal{K}_{\mathrm{st}}$, no matter a step is in a bunch or on the terrace, the velocity should be the same. On the other hand, as shown in Fig.5(b), step velocity shows an apparent inverse proportional relationship with the local slope, indicating that a step in a bunch slows down itself and will be caught by other steps coming from behind. Thus, the bunch grows larger. It is also noteworthy that the distribution of scatters changes over time in Fig.5(b). At the beginning stage, the variances of both the step velocities and the local slopes are minor. But during growth, both the two variances increase. The synchronous increases in variances indicate the mechanism of a surface loses its stability: Since the step velocities reversely depend on the local slopes, elementary steps collide ahead into bunches, resulting in higher step densities in bunches and lower on terraces. That results in step movements even slower in bunches and faster on terraces. Furthermore, again the slower moving bunches catch more steps from terraces. Step bunches intensify step bunching. That is why the surface roughness increases exponentially (shown in Fig.4).

3.2. Effect of $\mathcal{D}$

An enormous value for step kinetic coefficient, $\mathcal{K}_{\mathrm{st}}$, results in an enhancement in step bunching behavior. On the other hand, the diffusion coefficients are revealed to affect step bunching behavior in a reversed manner, as shown in Figure 6. Fig.6 shows the solutal concentration as a result of simulations using a pair of large and small values of both diffusion coefficient and step kinetic coefficient. The boundary condition is the same as the simulations carried out in the last section, but the crystal-solution boundary now has only one macrostep aggregated at the center of the surface (where the darkest part is located in the colormap in Fig.6) instead of steps distributed on the whole surface with different densities. We also calculated the relative step velocities with the solutal concentration on the crystal-solution boundary c^*_{st} with $v_{\mathrm{st}} = \mathcal{K}_{\mathrm{st}}(c^*_{\mathrm{st}} - c^*_{\mathrm{eq}})$. In the case of Fig.6(a) small $\mathcal{D}$ but large $\mathcal{K}_{\mathrm{st}}$, as analyzed in the last section, the solute are consumed by steps rapidly and can not be supplied in time by diffusion. Therefore, a low-concentration regime appeared around the macrostep, resulting in steps in the macrostep decelerated to a shallow level compared with the velocity of independent elementary step v^{∞}_{st} (eq. 17). In the two cases (b) large $\mathcal{D}$ and large $\mathcal{K}_{\mathrm{st}}$ (c) small $\mathcal{D}$ and

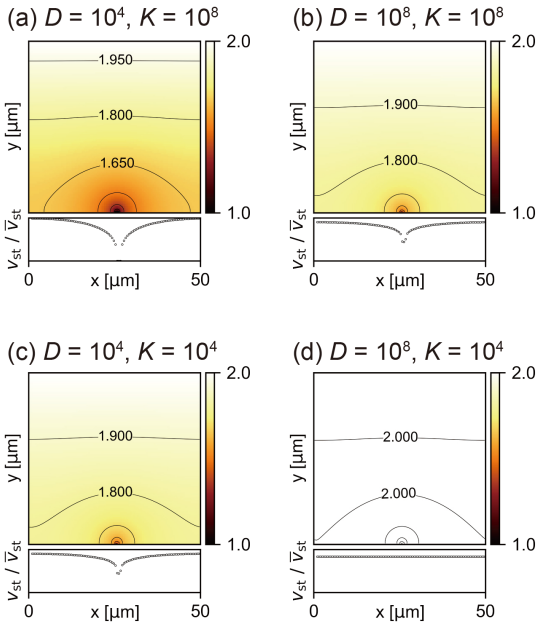

Figure 6: Solutal concentration and the relative step velocities simulated by CFD model with a macrostep at the center of the lower boundary. Only the diffusion coefficient and the step kinetic coefficient varied. The units for $\mathcal{D}$ is μm/s^2 and for $\mathcal{K}_{\rm st}$ is μm/s.

small $\mathcal{K}_{\rm st}$, the consumption of solute can be partially supplied by diffusion, thus the solute is less depleted arount the macrostep. We also found that the relative velocity is the same in the two cases. In contrast, in the last case (d) large $\mathcal{D}$ but small $\mathcal{K}_{\rm st}$, the solute consumption is entirely supplied by diffusion, and the solutal concentration difference is almost smoothed out, and the steps in macrosteps are no longer decelerated, which corresponds to the situation in Figure 5 (b).

3.3. Nondimensional Analysis of Growth Phase Map

According to Chernov,[37] in solution growth, step velocity of equally spaced steps on a vicinal surface can be written as

$$v_{\rm st}^{\infty} = \frac{\mathcal{K}_{\rm st} c_{eq} v_{\rm c} \sigma}{1 + \frac{a\mathcal{K}_{\rm st}}{\pi\mathcal{D}} \ln(\frac{x_0}{a} \sinh(\frac{\pi\delta}{x_0}))}, \tag{17}$$

where σ is the supersaturation degree at the maximum of boundary layer, a is the height of a elementary step, x_0 is the distance between two neighboring steps, δ is the thickness of boundary layer.

In most cases of solution growth, the boundary layer thickness is much larger than the step distance,

$$\pi\delta \gg x_0.$$

Therefore, the step velocity can be approximated as

$$v_{\mathrm{st}} \approx \frac{\mathcal{K}_{\mathrm{st}} c_{eq} v_{\mathrm{c}} \sigma}{1 + \frac{p\mathcal{K}_{\mathrm{st}}\delta}{\mathcal{D}}}, \tag{18}$$

where $p = a/x_0$.

While the reversed influences of step kinetics and diffusion have been elucidated in the last sections, according to equation 18, analysis of the balance between step kinetics and solute diffusion needs to be developed to provide a holistic picture. In this regard, we define a non-dimensional Damköhler number (D_a) for step-flow growth from solution as the ratio of reaction rate to diffusion rate and classify the observed regimes as a function of this number

$$D_a = \frac{p\mathcal{K}_{\mathrm{st}}\delta}{\mathcal{D}}, \tag{19}$$

where $p\mathcal{K}_{\mathrm{st}}$ is the "surface kinetic coefficient" reperesenting the incorporation rate of solute on the growth surface, δ is the characteristic length thus $\mathcal{D}/\delta$ is the characteristic diffusion velocity. Similar nondimensional numbers are defined and used as criteria of transition between stable growth and dendritic growth[38] or as an explanation of the growth rate profile in epitaxy of GaAs by MOCVD method[39]. $D_a \gg 1$ implies that the incorporation of growth units occurs mush faster than diffusion in solution. This leads to the diffusion limited growth regime since the solute consumed will not be supplemented in time. The step velocity can be approximated to

$$v_{\mathrm{st}} \approx \frac{\mathcal{D} c_{eq} v_{\mathrm{c}} \sigma}{p\delta}. \tag{20}$$

It makes sense since the steps will have to slow down to compensate for the decrease in solute concentration, which is more drastic near step bunching. For $D_a \ll 1$, the growth enters a kinetic limited regime, in which any consumption of solute will be supplemented immediately. Thus all steps will maintain the same velocity no matter where it is. The step velocity is then

$$v_{\mathrm{st}} \approx \mathcal{K}_{\mathrm{st}} c_{eq} v_{\mathrm{c}} \sigma. \tag{21}$$

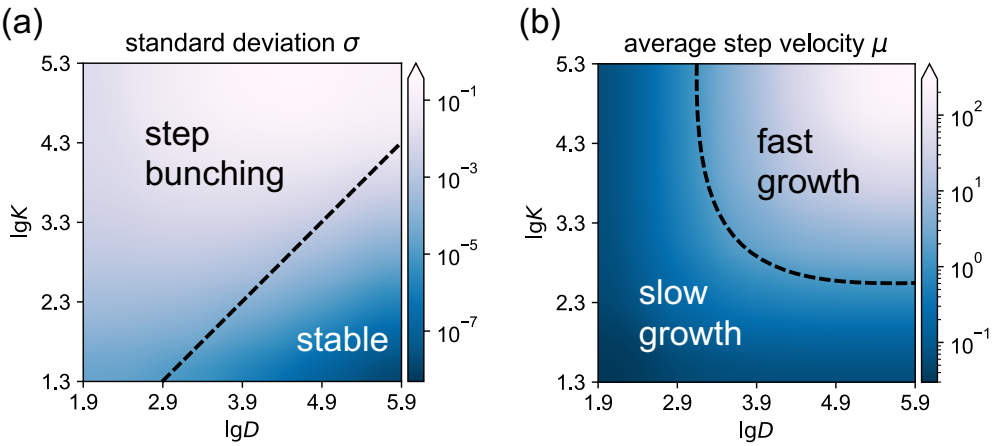

Figure 7: (a) Relative standard deviation of step velocity phase map and (b) average step velocity phase map as functions of Damköhler number. High Damköhler number leads to step bunching.

Figure 7(a) shows the two regimes mentioned above of step-flow growth as a function of the step kinetic coefficient and diffusion coefficient. Different values of the Damköhler number (D_a) are represented by the contour colors. As mentioned above, the transition from high to low Damköhler number results in the variation of growth mode from bunching to stable. It implies that a stable crystal growth process requests a large diffusion coefficient but a small step kinetic coefficient. On the other hand, Fig.7(b) shows the average step velocity as a function of the step kinetic coefficient and diffusion coefficient. Two regimes are divided by the contour line on which the step velocity reaches 1 μm s^{-1}, and the macroscopic crystal growth rate reaches 100 μm h^{-1}. With one of the independent variables, say, the diffusion coefficient fixed, the increase in step velocity by raising the step kinetic coefficient will meet a limitation, vice versa. Thus, to increase the growth rate, the large diffusion coefficient is still necessary, and the step kinetic coefficient must be raised as well.

The above discussion implies that the growth rate and surface morphology are partially a trade-off when designing solvent for crystal growth. Fortunately, there is an intersection between the fast growth regime and the stable growth regime, as shown in Figure 8. One can then refer to the intersection

as the "ideal regime", where both the growth rate and the morphology are acceptable.

3.4. Solvent design based on Damköhler number

By locating solvent on the phase map shown in Figure 8, we can figure out the "best" solvent for solution growth of SiC. To locate the solvent, one needs both the diffusion coefficient and the step kinetic coefficient values. The data of diffusion coefficient of substances is available from databases. While for the mixtures, the data of diffusion coefficient is obtained using the Stokes-Einstein equation.[40] The viscosity data is estimated with the unified equation developed by Kaptay et al.ref[41]. However, the step kinetic coefficient remains unknown due to a lack of knowledge of the interface and solvation energy. Therefore, instead of using the step kinetic coefficient, we first locate the solvent by the reported growth rates as a contour line. The intersection point between this contour line and a vertical line indicating the value of diffusion coefficient then is asserted as the location of solvent. Bearing in mind the arbitrariness of all the estimations, we located several reported solvents on the phase map, as shown in Fig.8. Since the reported cases have varied supersaturations, the step velocities are "normalized" by the supersaturations. The values of Si, $Si_{0.95}Ti_{0.05}$, $Si_{0.6}Cr_{0.4}$ and $Si_{0.56}Cr_{0.4}Al_{0.04}$ are typical values obtained in our previous experimental researches. While the values of $Si_{0.67}Al_{0.33}$ and $Si_{0.65}Ni_{0.31}Al_{0.04}$ are obtained from the report in which Onuma et al precisely measured the step velocities through an *in-situ* observation to the step movement.[19]

The coordinate of the solvents indicates that the solvent composition has a more negligible effect on the diffusion coefficient than on the step kinetic coefficient, and the elements reduce the diffusion coefficient without exception. Nickel and chromium improve the growth rate by increasing the step kinetic coefficients by almost an order of magnitude. People usually attribute the effect of improving growth rate to the increasing in carbon solubility. However, this study implies that these additive elements' modification of surface kinetics also contributes to the growth rate rise. On the other hand, the addition of aluminum decreases the step kinetic coefficient, stabilizing step bunching and decreasing step velocities.

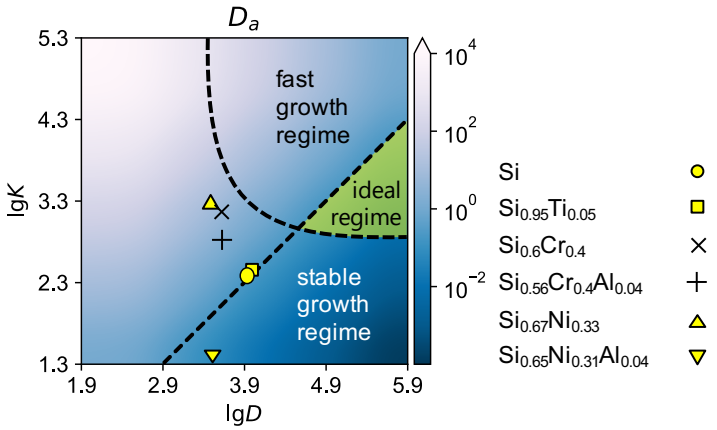

Figure 8: Phase map for solvent designing based on Damköhler number, several reported solvents are located on the phase map.

4. Conclusion

Solvent design involving reaction rate and transport phenomena rate is an approach to rapid and stable crystal growth. In this study, simulations are carried out about the influence of kinetic coefficient and diffusion rate on the step flow growth of the crystal.

1. The evolution behavior of surface roughness depends on the value of $\mathcal{K}_{\mathrm{st}}$. It is because the dependence of step velocity on the local slope will be changed by $\mathcal{K}_{\mathrm{st}}$, switching surface stability.
2. The dimensionless Damköhler number $D_a = p\mathcal{K}_{\mathrm{st}}\delta/D$ which determines the growth mode can be used as a criterion of intrinsic stability.
3. The ideal zone for both rapid and stable crystal growth requests for large $\mathcal{D}$ and moderate $\mathcal{K}_{\mathrm{st}}$.

Besides all the discussion above about the effect on step bunching behavior of the balance between step kinetics and mass transport, this study also reveals why supersaturation does not influence such step morphologies. As indicated by Mitani et al. [14]—changing supersaturation can only raise or lower step velocities in an aggregative manner, which do not affect the step velocity variance, thus no effect on step bunching behavior.

References

[1] T. Kimoto, Material science and device physics in SiC technology for high-voltage power devices, Japanese Journal of Applied Physics 54 (4) (2015) 040103. doi:10.7567/jjap.54.040103.

[2] J. Millan, P. Godignon, X. Perpina, A. Perez-Tomas, J. Rebollo, A Survey of Wide Bandgap Power Semiconductor Devices, IEEE Transactions on Power Electronics 29 (5) (2014) 2155–2163. doi:10.1109/tpel.2013.2268900.

[3] T. Kimoto, J. Cooper, Fundamentals of Silicon Carbide Technology: Growth, Characterization, Devices and Applications, Wiley, 2014.

[4] S. Harada, Y. Yamamoto, K. Seki, A. Horio, T. Mitsuhashi, M. Tagawa, T. Ujihara, Evolution of threading screw dislocation conversion during solution growth of 4H-SiC, APL Materials 1 (2) (2013) 022109. doi:10.1063/1.4818357.

[5] S. Harada, Y. Yamamoto, K. Seki, A. Horio, M. Tagawa, T. Ujihara, Different behavior of threading edge dislocation conversion during the solution growth of 4H–SiC depending on the Burgers vector, Acta Materialia 81 (2014) 284–290. doi:10.1016/j.actamat.2014.08.027.

[6] S. Harada, Y. Yamamoto, S. Xiao, M. Tagawa, T. Ujihara, Surface Morphology and Threading Dislocation Conversion Behavior during Solution Growth of 4H-SiC Using Al-Si Solvent, Materials Science Forum 778-780 (2014) 67–70. doi:10.4028/www.scientific.net/MSF.778-780.67.

[7] T. Ujihara, S. Kozawa, K. Seki, Alexander, Y. Yamamoto, S. Harada, Conversion Mechanism of Threading Screw Dislocation during SiC Solution Growth, Materials Science Forum 717-720 (2012) 351–354. doi:10.4028/www.scientific.net/MSF.717-720.351.

[8] Y. Yamamoto, S. Harada, K. Seki, A. Horio, T. Mitsuhashi, T. Ujihara, Effect of Surface Polarity on the Conversion of Threading Dislocations in Solution Growth, Materials Science Forum 740-742 (2013) 15–18. doi:10.4028/www.scientific.net/MSF.740-742.15.

[9] K. Murayama, T. Hori, S. Harada, S. Xiao, M. Tagawa, T. Ujihara, Two-step SiC solution growth for dislocation reduction, Journal of Crystal Growth 468 (2017) 874–878. doi:10.1016/j.jcrysgro.2016.11.100.

[10] D. Nakamura, I. Gunjishima, S. Yamaguchi, T. Ito, A. Okamoto, H. Kondo, S. Onda, K. Takatori, Ultrahigh-quality silicon carbide single crystals, Nature 430 (7003) (2004) 1009–1012. doi:10.1038/nature02810.

[11] K. Danno, H. Saitoh, A. Seki, H. Daikoku, Y. Fujiwara, T. Ishii, H. Sakamoto, Y. Kawai, High-Speed Growth of High-Quality 4H-SiC Bulk by Solution Growth Using Si-Cr Based Melt, Materials Science Forum 645-648 (2010) 13–16. doi:10.4028/www.scientific.net/MSF.645-648.13.

[12] H. Daikoku, M. Kado, H. Sakamoto, H. Suzuki, T. Bessho, K. Kusunoki, N. Yashiro, N. Okada, K. Moriguchi, K. Kamei, Top-Seeded Solution Growth of 4H-SiC Bulk Crystal Using Si-Cr Based Melt, Materials Science Forum 717-720 (2012) 61–64. doi:10.4028/www.scientific.net/MSF.717-720.61.

[13] M. Kado, H. Daikoku, H. Sakamoto, H. Suzuki, T. Bessho, N. Yashiro, K. Kusunoki, N. Okada, K. Moriguchi, K. Kamei, High-Speed Growth of 4H-SiC Single Crystal Using Si-Cr Based Melt, Materials Science Forum 740-742 (2013) 73–76. doi:10.4028/www.scientific.net/MSF.740-742.73.

[14] T. Mitani, N. Komatsu, T. Takahashi, T. Kato, K. Fujii, T. Ujihara, Y. Matsumoto, K. Kurashige, H. Okumura, Growth rate and surface morphology of 4H–SiC crystals grown from Si–Cr–C and Si–Cr–Al–C solutions under various temperature gradient conditions, Journal of Crystal Growth 401 (2014) 681–685. doi:10.1016/j.jcrysgro.2013.11.031.

[15] R. Janssen-van Rosmalen, P. Bennema, The role of hydrodynamics and supersaturation in the formation of liquid inclusions in KDP, Journal of Crystal Growth 42 (1977) 224–227. doi:10.1016/0022-0248(77)90198-1.

[16] T. Nishinaga, C. Sasaoka, K. Pak, Study of Nitrogen Inhomogeneity in LPE GaP by Spatially Resolved Photoluminescence, Japanese Journal of Applied Physics 28 (Part 1, No. 5) (1989) 836–840. doi:10.1143/JJAP.28.836.

[17] T. Mitani, N. Komatsu, T. Takahashi, T. Kato, S. Harada, T. Ujihara, Y. Matsumoto, K. Kurashige, H. Okumura, Effect of aluminum addition on the surface step morphology of 4H–SiC grown

from Si–Cr–C solution, Journal of Crystal Growth 423 (2015) 45–49. doi:10.1016/j.jcrysgro.2015.04.032.

[18] N. Komatsu, T. Mitani, Y. Hayashi, T. Kato, S. Harada, T. Ujihara, H. Okumura, Modification of the surface morphology of 4H-SiC by addition of Sn and Al in solution growth with SiCr solvents, Journal of Crystal Growth 458 (2017) 37–43. doi:10.1016/j.jcrysgro.2016.10.045.

[19] A. Onuma, S. Maruyama, N. Komatsu, T. Mitani, T. Kato, H. Okumura, Y. Matsumoto, Quantitative Analysis of Nanoscale Step Dynamics in High-Temperature Solution-Grown Single Crystal 4H-SiC via In Situ Confocal Laser Scanning Microscope, Crystal Growth & Design 17 (5) (2017) 2844–2851. doi:10.1021/acs.cgd.7b00325.

[20] S. Xiao, N. Hara, S. Harada, K. Murayama, K. Aoyagi, T. Sakai, T. Ujihara, Research on Solvent Composition for Different Surface Morphology on C Face during 4H-SiC Solution Growth, Materials Science Forum 821-823 (2015) 39–42. doi:10.4028/www.scientific.net/MSF.821-823.39.

[21] S. Xiao, S. Harada, K. Murayama, M. Tagawa, T. Ujihara, Conversion Behavior of Threading Screw Dislocations on C Face with Different Surface Morphology During 4H-SiC Solution Growth, Crystal Growth & Design 16 (11) (2016) 6436–6439. doi:10.1021/acs.cgd.6b01107.

[22] X. Liu, C. Zhu, S. Harada, M. Tagawa, T. Ujihara, Application of C-face dislocation conversion to 2 inch SiC crystal growth on an off-axis seed crystal, CrystEngComm (2019) 10.1039.C9CE01338Edoi:10.1039/C9CE01338E.

[23] J. J. De Yoreo, L. A. Zepeda-Ruiz, R. W. Friddle, S. R. Qiu, L. E. Wasylenki, A. A. Chernov, G. H. Gilmer, P. M. Dove, Rethinking Classical Crystal Growth Models through Molecular Scale Insights: Consequences of Kink-Limited Kinetics, Crystal Growth & Design 9 (12) (2009) 5135–5144. doi:10.1021/cg900543g.

[24] R. I. Ristic, J. J. DeYoreo, C. M. Chew, Does Impurity-Induced Step-Bunching Invalidate Key Assumptions of the Cabrera-Vermilyea Model?, Crystal Growth & Design 8 (4) (2008) 1119–1122. doi:10.1021/cg7010474.

[25] T. Mitani, K. Naoyoshi, K. Tomohisa, Variations of macrostep structures with solvent compositions in 4H-SiC solution growth, Journal of the Japanese Association for Crystal Growth 45 (2) (2018). doi:10.19009/jjacg.3-45-2-02.

[26] P. G. Vekilov, H. Lin, F. Rosenberger, Unsteady crystal growth due to step-bunch cascading, Physical Review E 55 (3) (1997) 3202–3214. doi:10.1103/PhysRevE.55.3202.

[27] Y.-I. Kwon, B. Dai, J. J. Derby, Assessing the dynamics of liquid-phase solution growth via step growth models: From BCF to FEM, Progress in Crystal Growth and Characterization of Materials 53 (3-4) (2007) 167–206. doi:10.1016/j.pcrysgrow.2007.09.001.

[28] M. Inaba, M. Sato, Effect of Flow in Solution on Motion of Steps during Solution Growth, Journal of the Physical Society of Japan 80 (7) (2011). doi:10.1143/jpsj.80.074606.

[29] I. V. Markov, Crystal Growth for Beginners: Fundamentals of Nucleation, Crystal Growth and Epitaxy, 3rd Edition, World Scientific, New Jersey, 2016.

[30] G. G. Gnesin, A. I. Raichenko, Kinetics of the liquid-phase reactive sintering of silicon carbide, Soviet Powder Metallurgy and Metal Ceramics 12 (5) (1973) 383–389. doi:10.1007/BF00791264.

[31] R. I. Scace, G. A. Slack, Solubility of Carbon in Silicon and Germanium, The Journal of Chemical Physics 30 (6) (1959) 1551–1555. doi:10.1063/1.1730236.

[32] W.-K. Burton, N. Cabrera, F. Frank, The growth of crystals and the equilibrium structure of their surfaces, Philosophical Transactions of the Royal Society of London. Series A, Mathematical and Physical Sciences 243 (866) (1951) 299–358.

[33] A. A. Chernov, How does the flow within the boundary layer influence morphological stability of a vicinal face?, Journal of Crystal Growth 118 (3-4) (1992) 333–347. doi:10.1016/0022-0248(92)90080-3.

[34] A. A. Chernov, S. R. Coriell, B. T. Murray, Morphological stability of a vicinal face induced by step flow, Journal of Crystal Growth 132 (3-4) (1993) 405–413. doi:10.1016/0022-0248(93)90065-5.

[35] S. R. Coriell, B. T. Murray, A. A. Chernov, G. B. McFadden, Step bunching on a vicinal face of a crystal growing in a flowing solution, Journal of Crystal Growth 169 (4) (1996) 773–785. doi:10.1016/s0022-0248(96)00470-8.

[36] M. Uwaha, Introduction to the BCF theory, Progress in Crystal Growth and Characterization of Materials 62 (2) (2016) 58–68. doi:10.1016/j.pcrysgrow.2016.04.002.

[37] A. Chernov, The spiral growth of crystals, Physics-Uspekhi 4 (1) (1961) 116–148.

[38] X. Li, J. Glimm, X. Jiao, C. Peyser, Y. Zhao, Study of crystal growth and solute precipitation through front tracking method, Acta Mathematica Scientia 30 (2) (2010) 377–390. doi:10.1016/S0252-9602(10)60055-0.

[39] H. Oh, M. Sugiyama, Y. Nakano, Y. Shimogaki, Surface reaction kinetics in metalorganic vapor phase epitaxy of GaAs through analyses of growth rate profile in wide-gap selective-area growth, Japanese journal of applied physics 42 (10R) (2003) 6284.

[40] A. Einstein, On the motion of small particles suspended in liquids at rest required by the molecular-kinetic theory of heat, Annalen der physik 17 (549-560) (1905) 208.

[41] G. Kaptay, A unified equation for the viscosity of pure liquid metals, Zeitschrift für Metallkunde 96 (1) (2005) 24–31. doi:10.3139/146.018080.